Steel and Composite Structures, *Vol. 30, No. 5 (2019) 483-492*
DOI: https://doi.org/10.12989/scs.2019.30.5.483

Lateral torsional buckling of steel I-beams: Effect of initial geometric imperfection

Selcuk Bas*

Department of Civil Engineering, Faculty of Engineering, Bartin University, 74100 Bartin, Turkey

(*Received November 7, 2018, Revised March 5, 2019, Accepted March 8, 2019*)

Abstract. In the current study, the influence of the initial lateral (sweep) shape and the cross-sectional twist imperfection on the lateral torsional buckling (LTB) response of doubly-symmetric steel I-beams was investigated. The material imperfection (residual stress) was not considered. For this objective, standard European IPN 300 beam with different unbraced span was numerically analyzed for three imperfection cases: (i) no sweep and no twist (perfect); (ii) three different shapes of global sweep (half-sine, full-sine and full-parabola between the end supports); and (iii) the combination of three different sweeps with initial sinusoidal twist along the beam. The first comparison was done between the results of numerical analyses (FEM) and both a theoretical solution and the code lateral torsional buckling formulations (EC3 and AISC-LRFD). These results with no imperfection effects were then separately compared with three different shapes of global sweep and the presence of initial twist in these sweep shapes. Besides, the effects of the shapes of initial global sweep and the inclusion of sinusoidal twist on the critical buckling load of the beams were investigated to unveil which parameter was considerably effective on LTB response. The most compatible outcomes for the perfect beams was obtained from the AISC-LRFD formulation; however, the EC-3 formulation estimated the P_{cr} load conservatively. The high difference from the EC-3 formulation was predicted to directly originate from the initial imperfection reduction factor and high safety factor in its formulation. Due to no consideration of geometric imperfection in the AISC-LFRD code solution and the theoretical formulation, the need to develop a practical imperfection reduction factor for AISC-LRFD and theoretical formulation was underlined. Initial imperfections were obtained to be more influential on the buckling load, as the unbraced length of a beam approached to the elastic limit unbraced length (L_r). Mode-compatible initial imperfection shapes should be taken into account in the design and analysis stages of the I-beam to properly estimate the geometric imperfection influence on the P_{cr} load. Sweep and sweep–twist imperfections led to 10% and 15% decrease in the P_{cr} load, respectively, thus; well-estimated sweep and twist imperfections should considered in the LTB of doubly-symmetric steel I-beams.

Keywords: lateral torsional buckling; initial geometric imperfection; doubly-symmetric steel I-beam; finite element model

1. Introduction

Due to higher slenderness of steel structures, the stability considerations to mitigate the effects of buckling problem become more significant in the design philosophy of steel structures. Geometric imperfection generally resulting from manufacturing, construction, storage and shipping is an additional critical point to be considered, which makes structural steel elements more vulnerable to buckling. The flexural capacities of steel I-beams depend on four different limits states: (i) Yielding (plastic failure); (ii) Local (web and flange) buckling (LB); (iii) Lateral torsional buckling (LTB); (iv) Lateral distortional buckling (LDB). As depicted in Fig. 1, the last three of them (LB, LTB and LDB) are pertinent to stability problems of steel beam. A steel girder is capable of resisting moments as high as its full flexural capacity (plastic moment capacity), if these three forms of buckling (LB, LTB and LDB) can be prevented by various means (lateral braces, transverse and longitudinal web stiffeners, presence of a slab on top of the beam, etc.). LB corresponds to the plate buckling of the individual components (web or flange) with no lateral bending and twisting rotations of the beam. LTB; on the other hand, corresponds to the buckling of the beam as a whole without any distortion in the web and flange plates, i.e., no local buckling. In LTB, the compression side of a beam tends to undergo flexural (Euler) or flexural-torsional buckling about the minor axis, while the tension side tends to remain stable. The differential tendencies of the two sides result in beam rotations about the longitudinal axis, as well as lateral bending of the beam. Hence, coupled lateral bending deformations and twisting rotations take place in LTB. Finally, LDB is called to be a combination of LTB and web buckling. Unlike LTB, the web plate buckles and distorts in LDB in addition to the overall buckling of the beam.

Stability of steel beams, and thus these three modes of buckling are affected by the initial imperfections markedly. The initial imperfections of steel members can be categorized into two major groups as material imperfections (residual stresses, etc.) and geometrical imperfections. Steel girders in a finished superstructure might possess three

*Corresponding author, Ph.D., Assistant Professor,
E-mail: sbas@bartin.edu.tr

http://www.techno-press.org/?journal=scs&subpage=6
ISSN: 1229-9367 (Print), 1598-6233 (Online)

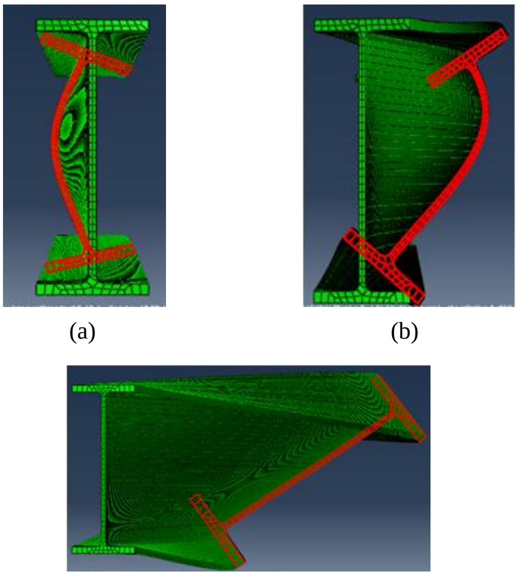

(a) (b)

(c)

Fig. 1 Buckling types of I-beam: (a) LB (web); (b) LDB; (c) LTB (Bas *et al*. 2016)

different types of initial geometric imperfections, namely the vertical (in-plane) imperfection (camber), the lateral (out-of-plane) imperfection (sweep) and the initial angle of twist. Camber mainly affects the vertical deformations of a girder in the prebuckling stage (prior to bifurcation). The in-plane flexural deformations up to buckling have rather minor influence on the buckling moments and buckling behavior of flexural members, particularly if the major-axis flexural rigidity of a member is much higher than its minor-axis flexural rigidity. In steel I-girders, the difference between the major-axis (in-plane) and minor-axis (out-of-plane) flexural rigidities is generally so significant that the in-plane deformations in the pre-buckling stage, and hence the camber can be totally neglected in the buckling analyses. The second and third forms of initial geometric imperfection (sweep and twisting angle), on the contrary, do have a deep impact on the buckling behavior of flexural members.

Many investigations in literature have continuously focused on the lateral torsional buckling behavior of steel beams. In addition, various important structural steel codes, including AISC-LRFD (2016), Eurocode-3 (2005) and AS4100-1998 (2016) pay special attention to stability problems pertinent to buckling of steel structures. However, limited studies were conducted in literature on how initial geometric imperfections affect the lateral torsional buckling response of doubly-symmetric steel I-beam. A practical approach to predicting the location of buckling and the bending capacity of slender tubes was developed by Mirzaie *et al*. (2018) proposing a new measure of geometric imperfection. Based on the verification of a newly developed approach with the experiments on eight large-scale slender tubes, they intended to quantify the effect of imperfection on the buckling behavior of such slender tubes. Patch laoding resistance of girders stiffened in longitudinal direction was studied in the study of Kövesdi *et al*. (2018). In that study, the first eigen modes were obtained as suitable imperfection shapes for safe resistances. Dou *et al*. (2018) made extensive numerical analyses on inelastic lateral flexural buckling of uniaxially loaded columns to specify their restraint stiffness and strength requirements considering the random imperfections. They demonstrated that for accurately estimating the restraint force, full restraining stiffness approach was more suitable than the traditional estimation ignoring random imperfections. Beyer *et al*. (2018) studied the effects of geometric imperfections on hot-rolled U-shaped members. They made certain recommendations on the form and amplitude properties of geometric imperfection and material imperfection of residual stresses. The effects of half sine wave and other possible buckling mode geometrical imperfection shapes on flexural inelastic buckling strength of columns with evenly located lateral braces were estimated performing FE analysis by Dou and Pi (2016). Eigen buckling results from the theoretical geometric imperfections were also compared to the buckling results obtained for the statistical geometric imperfections based on the measurements in laboratory. Thus, the most critical geometric imperfection shape was presented in Dou *et al*. (2018) to reliably make an advanced inelastic buckling analysis for laterally braced columns. The ultimate buckling load capacities of beams and columns with a flexible restraint at the mid-span was predicted in the study of Unterweger *et al*. (2017) through geometrically and materially non-linear analyses (GMNIA). In this study, the first mode geometric imperfection was interestingly determined to be an increasing buckling load parameter when compared to the beam with rigid restraint. A study on the reasons for the finite element analysis (FEA) of I-sections yielding to smaller lateral torsional buckling (LTB) moment values than the AISC/AASHTO LTB equations was conducted by Subramanian and White (2017). They recommended certain improvements to the formulations given in the codes. A set of investigations on stability problem were carried out by Kala (2013, 2017), Kala and Valeš (2017) and Kala *et al*. (2017). In those studies, inelastic FE analyses on lateral buckling of beam elements, global sensitivity analysis of LTB according to FE analysis results and the effect of initial random imperfection on the stability of truss system were studied. Another random initial imperfection was considered by Chen *et al*. (2016) to estimate the load carrying capacity of shell structures or shell-like space frames. They determined the main statistical characteristics of the random imperfection model according to measurements obtained from real reticulated shell structures. Agüero *et al*. (2015) made an investigation on the approach presented in EN 1993-1-1 (EC-3) to refine the provisions of the code for the magnitude of the geometric equivalent imperfection. They recommended to consider higher buckling modes as geometric imperfection. With regard to different boundary conditions and geometric imperfections, Dahmani and Boudjemia (2014) and Nguyen *et al*. (2013) made similar studies on steel and pultruded FRP I-beam, respectively. They showed that FE modeling methodology was effective for parametric analysis on lateral torsional buckling of beam element.

Recent other studies in the literature accounted for the influence of the different initial geometric imperfections on the buckling response of steel beams and columns to a limited extent. In these studies, buckling response was investigated in terms of different aspects of design and numerical modeling. Thai *et al*. (2017) improved the generalized plastic hinge analysis taking the local and lateral torsional buckling modes into account. Flexural strength degradation owing to the buckling effects was calculated in that study with the well-known LRFD formulations. Buckling restrained braced frames were analyzed under the earthquake motion by Roy *et al*. (2015) as a limiting tool for adapting torsional eccentricity of steel buildings with four storey. Aydin *et al*. (2015) made an effort in their study to determine critical buckling loads of prismatic steel beams with I-section. They proposed new analytical and design procedures for lateral buckling of prismatic steel beams using energy approach. Similarly, considering the potential energy assumption, Kuś (2015) developed an approach to attain critical lateral torsional buckling (LTB) of beams with tapered section. For this aim, he conducted parametric analyses on LTB of the beams with simultaneously tapered flanges and web and revealed that tapering of the flanges was more crucial than tapering of the web. Many other studies in the literature (Mohebkhah 2004, Zirakian 2008, Kalkan and Buyukkaragoz 2012, Zirakian and Zhang 2012, Naderian *et al*. 2014, Pezeshky and Mohareb 2014, Hassan and Mohareb 2015, Sonck and Belis 2015, Yang *et al*. 2016, Zhou *et al*. 2016, Lei and Li 2017, Subramanian and White 2017, Winkler *et al*. 2017, Tankov *et al*. 2018, Tohidi and Sharifi 2018) took the influence of geometrical imperfections on LTB response of structural members into account.

The above-mentioned literature survey indicates that the effects of the initial out-of-plane shape of the longitudinal axis of a beam and its twist along the span on LTB have not been studied in the literature. Most of the previous researchers investigated the influence of the magnitude of initial geometric imperfections on LTB response. To understand the main idea behind the present study, the differences between the LTB behavior of an initially imperfect beam and a perfect beam should be explained. A steel I-girder with lateral imperfections has a completely different buckling behavior compared to its initially perfect counterpart. Unlike the bifurcation type of buckling in geometrically perfect steel beams, the beams with sweep and twist exhibit a “limit-load type of buckling”. Sweep and twist cause a beam to undergo lateral deformations from the start of loading and an initially imperfect beam buckles at a limit load lower than the critical load of its perfect configuration after excessive lateral deformations along the course of loading. The difference between the limit load of a beam with sweep and the critical buckling (bifurcation) load of its perfect counterpart depends on the magnitude of sweep and twist in the first place. The present study, on the other hand, tries to answer another important question of whether the shape of the initial lateral bow influences the buckling load and the buckling behavior of a beam, or not. The main idea behind the study is based on the fact that the flexural (Euler) or flexural-torsional buckling transforms a compression member with end supports to a half-sine wave between the ends. In other words, the buckling deformations are distributed in a sinusoidal manner from 0 at supports to a maximum at mid-span. LTB is a type of column buckling, since the compression side of a beam behaves as a compression member and undergoes buckling if not supported adequately. Therefore, both the lateral deformations and twist rotations in a beam follow a half-sinusoidal pattern between the ends in LTB, as well. Theoretically, the resistance of a beam to LTB and the buckling load are expected to decrease as the initial lateral bow is closer to a half-sine wave.

In this respect, the present study investigates the relationship between the closeness of the initial sweep shape with or without cross-sectional twist to a half-sine wave and the buckling load of doubly-symmetric steel

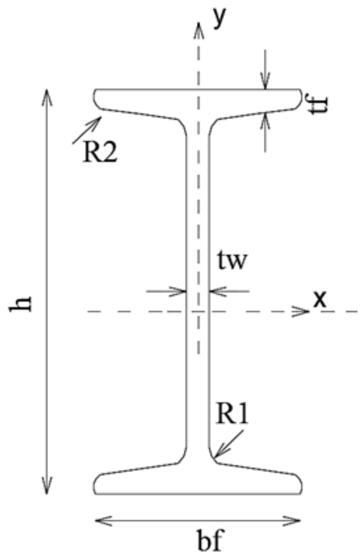

A: Section Area	6900 mm^2
h: Depth of cross-section	300 mm
b_f: Width of cross-section	125 mm
t_f: Flange thickness	16.2 mm
t_w: Web thickness	10.8 mm
R_1: Fillet radius of web	11.00 mm
R_2: Fillet radius of flange	6.5 mm
I_x: Moment of inertia aboutthe x- axis	98 x 10^6 mm^4
I_y: Moment of inertia about the y- axis	451 x 10^4 mm^4
i_x: Radius of gyration about the x- axis	119 mm
i_y: Radius of gyration about the y- axis	25.6 mm
S_x: Section modulus about the x- axis	653 x 10^3 mm^3
S_y: Section modulus about the y- axis	72.2 x 10^3 mm^3
W_{px}: Plastic section modulus about the x- axi	762 x 10^3 mm^3
W_{py}: Plastic section modulus about the y- axi	121 x 10^3 mm^3
J: Torsional constant	56.8 x 10^4 mm^4
C_w: Warping constant	91.8 x 10^9 mm^6
E: Modulus of elasticity	2 x 10^5 MPa
ν: Poisson's ratio	0.3
G: Shear modulus	7.692 x 10^4 MPa
F_y: Yield stress	275 MPa

Fig. 2 Geometrical and material properties of IPN300

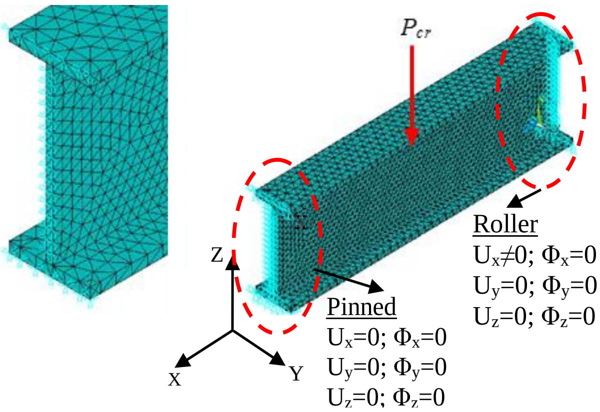

Fig. 3 Boundary and loading condition of IPN300

I-beams. Three different shapes of sweep, namely the half-sine wave, a complete parabola and a full-sine wave between the end supports were adopted together with the analyses on reference beams, i.e., beams with no initial geometric imperfections. In an effort to verify the accuracy of the FE results, the results of numerical analyses on reference beams were first compared to the analytical estimates from a theoretical solution and the code LTB formulations (EC3 and AISC-LRFD). Later, the FE analysis results of beams with no imperfections were compared to the respective values of the beams with three different shapes of global sweep both in the presence and absence of initial twist. In this way, the effects of initial global sweep shapes and the inclusion of sinusoidal twist on the critical buckling load (P_{cr}) was tried to be unveiled.

2. Numerical study

The standard European IPN300 beam, whose geometrical and material details are given in Fig. 2, was adopted in the analyses. The ABAQUS (2017) FEA software was used in the numerical stage. For this objective, C3D20R solid element with 20-node quadratic brick and reduced integration properties were used by also considering the fillets at the web-flange interfaces and the unstiffened (free) ends of the flanges. Free meshing approach was adapted with the meshed element size of less than 10 mm.

As demonstrated in Fig. 3, the beams were simply supported in and out of plane at the ends. In other words, the lateral and vertical deformations of the beam ends were prevented. Furthermore, lateral support was provided along the entire beam height at the support locations to restrain the twisting rotations. One of the most significant concerns in the buckling analyses of I-beams is the restraint against warping deformations at beam-ends. I-beams undergo significant warping deformations under major-axis bending moments. If these deformations are prevented at the supports, the buckling moments increase considerably. In the present FE analysis, the longitudinal deformations were allowed all along the beam height at the roller-supported end, yet only the longitudinal displacement was restrained at the pinned-supported end. In this way, the beam was

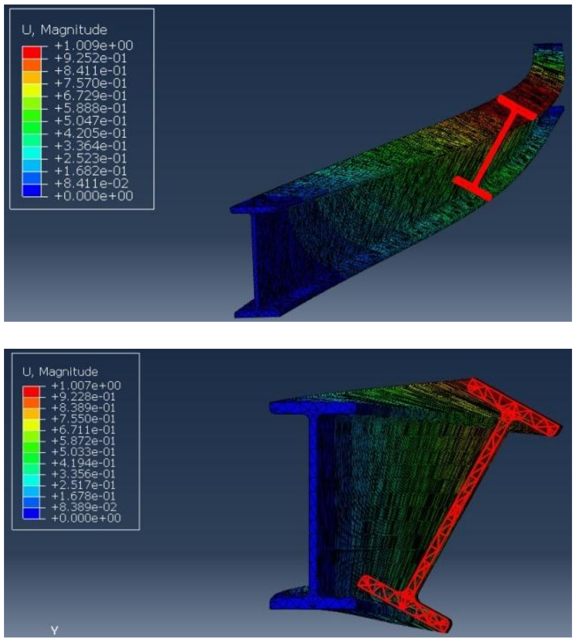

Fig. 4 General views from the 1st bucklingmode of FE model of IPN300 beam with the length of L = 10 m

allowed to undergo free warping deformations. The beams were subjected to concentrated loading at mid-span. The load was applied on top of the beam to simulate the actual loading conditions in practice. The destabilizing effect of the load location with respect to the shear center of the section was also considered in the analytical study. General view from the 3-D FE model of IPN300 beam is depicted in Fig. 4. The geometric sweep imperfections of full-sine, half-sine and full-parabola as well as sinusoidal twist imperfection were considered in the buckling analysis with large-deflection option of the ABAQUS (2017) FEA.

Steel IPN 300 girders with different un-braced lengths were analyzed in the present study. The beams with no initial geometric imperfections were denoted as the reference beams. The unbraced lengths of the reference beams were chosen in a way that all reference beams were ensured to undergo elastic LTB. In other words, none of the reference beams yielding was allowed to initiate before buckling. In this way, influence of the material behavior was tried to be minimized in the buckling analyses. Steel grade of S275 was considered for numerical and analytical analysis. The un-braced lengths of the analyzed beams are 6.0, 6.5, 7.0, 7.5, 8.0, 8.5, 9.0, 9.5 and 10.0 meters, which exceed the limiting laterally unbraced length for the limit state of inelastic LTB, i.e., the elastic limit length (L_r), calculated from the AISC-LRFD (2016) equation (Eq. (1))

$$L_r = 1.95 \cdot r_{ts} \cdot \frac{E}{0.7 \cdot F_y} \cdot \sqrt{\frac{J \cdot c}{S_x \cdot h_o}} \cdot \sqrt{1 + \sqrt{1 + 6.76 \cdot \left(\frac{0.7 \cdot F_y}{E} \cdot \frac{S_x \cdot h_o}{J \cdot c} \right)^2}} \tag{1}$$

where;

r_{ts}: effective radius gyration of the section in mm, E: the modulus of elasticity of steel (200 GPa), F_y: the yield stress (275 MPa), J: the torsional constant, S_x: the elastic section modulus with respect to the horizontal principal axis, h_o: the distance between the flange centroids in mm. The term "c" in Eq. (1) is simply taken equal to 1.0 for I sections. As defined above, r_{ts} is the radius of gyration of the effective area of the section, which encompasses the entire compression flange and one-sixth of the web and it can be calculated from the following simplified formula of Eq. (2) for I-beams according to AISC-LRFD (2016)

$$r_{ts} = \frac{b_f}{\sqrt{12 \cdot \left(1 + \frac{1}{6} \cdot \frac{h \cdot t_w}{b_f \cdot t_f}\right)}} \tag{2}$$

where, b_f: the flange width, t_f :the flange thickness, t_w: the web thickness, h: the clear distance between flanges.

The L_r value for the IPN 300 section was calculated as 5.56 m from Eq. (1) and then the smallest unbraced length of the analyzed beams was chosen as 6.0 m to guarantee complete elastic LTB. Thus, as stated above, FE analysis was performed for the beam having unbraced length of 6.0, 6.5, 7.0, 7.5, 8.0, 8.5, 9.0, 9.5 and 10.0 meters. The FE analysis software ABAQUS was utilized in the analyses. The reference beams, i.e., the beams with no sweep and twist, were analyzed with the help of the "eigenvalue buckling analysis" tool of the software. Three different groups of imperfect beams with or without sinusoidal twist were analyzed for identical unbraced lengths with the reference beams. The sweep shapes of the imperfect analyzed beams are as follows and these sweep imperfection were depicted schematically in Fig. 5:

- Half-sine wave between the supports (zero at the supports and maximum at mid-span) with the formulation given in Eq. (3)

$$u = u_0 \cdot \sin(\frac{\pi x}{L_b}) \tag{3}$$

- A complete parabola between the supports (zero at the supports and maximum at mid-span) with the formulation given in Eq. (4)

$$u = \frac{1}{250}(x - \frac{x^2}{L_b}) \tag{4}$$

- Full-sine wave between supports (zero at the supports and mid-span and maximum at quarter points on the span) with the formulation given in Eq. (5)

$$u = u_0 \cdot \sin(\frac{2\pi x}{L_b}) \tag{5}$$

where, u_0: amplitude (maximum value) of sweep in mm, L_b: unbraced length in mm

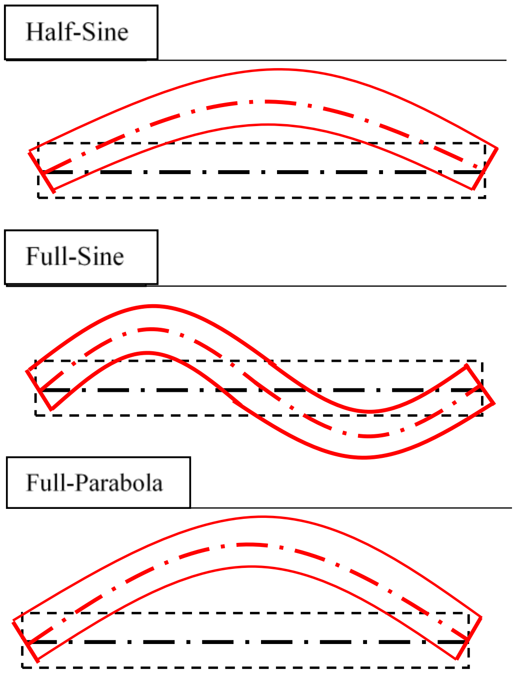

Fig. 5 Schematic presentation of sweep imperfections

The maximum sweep value (u_0) was identical for all the three cases, which was taken as $u_0 = L_b/1000$. L_b corresponds to the distance between the end supports, i.e., the unbraced length. The variation of sectional twist with the amplitude of ϕ_0 = L_b/(2000h) is also given in Eq. (6) for all three shapes of sweep

$$\phi = \phi_0 \cdot \sin(\frac{\pi x}{L_b}) \tag{6}$$

where, ϕ_0: amplitude of twist angle in rad, L_b: unbraced length in mm. The initial twisting angle of the beams was adjusted in such a way that the top flange of a beam has greater lateral imperfection compared to the bottom flange. In this way, the initial twisting angle has an additional decreasing effect on the buckling load in addition to the reduction associated with the sweep along the beam longitudinal axis.

3. Analytical study

The buckling moments of the analyzed beams were compared to the analytical estimates from the AISC-LRFD (2016) specification and Eurocode-3 (2005) LTB solutions and the theoretical formulation proposed by SSRC (2010). The elastic LTB moment (M_n) can be calculated from the following formula Eq. (7), according to the AISC-LRFD (2016) specifications

$$M_n = \left[\frac{C_b \cdot \pi^2 \cdot E}{\left(\frac{L_b}{r_{ts}}\right)^2} \cdot \sqrt{1 + 0.078 \cdot \frac{J \cdot c}{S_x \cdot h_o} \cdot \left(\frac{L_b}{r_{ts}}\right)^2} \right] \cdot S_x \tag{7}$$

where, C_b is the lateral-torsional buckling modification factor for non-uniform moment diagrams when both ends of the unsupported segment are braced, obtained from the following equation Eq. (8)

$$C_b = \frac{12.5 \cdot M_{\max}}{2.5 \cdot M_{\max} + 3 \cdot M_A + 4 \cdot M_B + 3 \cdot M_C} \cdot R_m \leq 3 \qquad (8)$$

where, M_{max} is the absolute value of the maximum moment in the unbraced segment in kNm; M_A, M_B and M_C refer to the absolute values of the bending moment at quarter point, centerline and three-quarter point of the unbraced segment in kN.m, respectively. The term R_m is denoted as the cross-section mono-symmetry parameter and it is taken equal to 1.0 for doubly-symmetric I-beams. The mid-span concentrated loading and simple support conditions at the ends create a bending moment diagram with a C_b value of about 1.32, implying that the buckling moments of the analyzed beams were about 32% higher than an identical beam with a uniform bending moment along the span.

$$M_n = \chi_{LT\,\mathrm{mod}} \cdot W_y \cdot F_y \qquad (9)$$

$$\chi_{LT,\mathrm{mod}} = \frac{\chi_{LT}}{f};\ \chi_{LT,\mathrm{mod}} \leq 1.0$$

$$f = 1 - 0.5(1-k_c)\left[1 - 2.0\left(\bar{\lambda}_{LT} - 0.8\right)^2\right];\ f \leq 1.0$$

$$\chi_{LT} = \frac{1}{\Phi_{LT} + \sqrt{\Phi^2_{LT} - \beta\bar{\lambda}^2_{LT}}},\ \begin{cases} \chi_{LT} \leq 1.0 \\ \chi_{LT} \leq \dfrac{1}{\bar{\lambda}^2_{LT}} \end{cases} \qquad (10)$$

$$\bar{\lambda}_{LT} = \left[\frac{W_y f_y}{M_{cr}}\right]^{0.5};\ M_{cr} = \frac{\pi}{L_b}\sqrt{GJ \cdot EI_y\left(1 + \frac{\pi^2 EI_w}{L_b{}^2 GJ}\right)}$$

$$\Phi_{LT} = 0.5\left[1 + \alpha_{LT}\left(\bar{\lambda}_{LT} - \bar{\lambda}_{LT,0}\right) + \beta\bar{\lambda}^2_{LT}\right]$$

$$\bar{\lambda}_{LT,0} \leq 0.4;\ \beta \geq 0.75$$

LTB moment estimates are obtained with this simplification. The elastic LTB solution (Eq. (9)) of EC3 (1995) is a little more complicated and detailed compared to the AISC-LRFD (2016) LTB solution. The input parameters of the Eq. (9) are also given with Eqs. (10). In Eqs. (10), $\chi_{LT,mod}$: a modification factor for LTB, accounting for the non-uniform moment distribution between the braces (similar to C_b in the AISC-LRFD solution), χ_{LT}: reduction factor, α_{LT}: imperfection factor, k_c: correction factor for moment distribution, f: modification factor for χ_{LT}, $\bar{\lambda}_{LT}$: non-dimensional slenderness for LTB, Φ_{LT}: value to determine the reduction factor χ_{LT} and γ_{M1}: the safety factor for the limit state of LTB.

A rather generic form of the lateral torsional buckling moment equation for steel beams was presented in SSRC (2010) with Eq. (11)

$$M_n = C_b \frac{\pi}{L_b} \cdot \sqrt{E \cdot I_y \cdot G \cdot J} \cdot \sqrt{1 + \frac{\pi^2}{L_b^2} \cdot \frac{E \cdot C_w}{G \cdot J}} \qquad (11)$$

The factor C_b in this equation accounts for the loading and support conditions of the beam (non-uniform moment distribution along the span) and the location of the load with respect to the shear center of the section. C_b can be obtained from the following Eq. (12)

$$C_b = A \cdot B^{2 \cdot y / h} \qquad (12)$$

where, y: the distance from the mid-height of the section to the load application point, h: the entire depth of the section (300 mm). The constants A and B are taken as 1.35 and (1-0.180.W^2 + 0.649W), respectively, for a simply-supported beam with concentrated mid-span loading. This equation given in SSRC (2010) is estimated to yield to elastic LTB moment value within 5% accuracy with respect to the test results. Considering the calculation of the maximum bending moment (M_{max}) for simply-supported beam with a concentrated load at mid-point, the critical buckling load (P_{cr}) was found with the help of Eq. (13)

$$P_{cr} = \frac{4 \cdot M_n}{L_b} \qquad (13)$$

Table 1 Comparison between FE and analytical formulations (AISC-LRFD, EC3 and SSRC 2010)

Unbraced length (m)	Reference (FE) $P_{cr,\mathrm{FE}}$	Buckling load (P_{cr}, t) AISC-LRFD (2016) $P_{cr,\mathrm{AISC}}$	$P_{cr,\mathrm{AISC}}/P_{cr,\mathrm{FE}}$ (%)	EC-3 (2005) $P_{cr,\mathrm{EC3}}$	$P_{cr,\mathrm{EC3}}/P_{cr,\mathrm{FE}}$ (%)	SSRC (2010) $P_{cr,\mathrm{SSRC}}$	$P_{cr,\mathrm{SSRC}}/P_{cr,\mathrm{FE}}$ (%)
6.0	8.83	9.28	105	6.99	79	8.40	95
6.5	7.64	7.84	103	6.09	80	7.18	94
7.0	6.72	6.71	100	5.30	79	6.22	92
7.5	5.91	5.82	99	4.73	80	5.44	92
8.0	5.27	5.09	97	4.20	80	4.80	91
8.5	4.70	4.49	96	3.78	80	4.27	91
9.0	4.28	7.00	93	3.43	80	3.82	89
9.5	3.89	3.58	92	3.13	80	3.44	88
10.0	3.56	3.22	91	2.86	81	3.12	88

4. Results and comparison

4.1 Numerical and analytical results

In an effort to prove the accuracy of the FE modeling considerations including mesh size, boundary and load conditions, analysis options etc., eigenvalue buckling analysis was conducted for each perfect beam. For this aim, the results obtained from the FE analyses of the perfect beams were compared to the analytical estimates (Fig. 6) and the percent differences between the numerical and analytical results were set forth (Table 1).

Besides, the variation of the results from the theoretical (SSRC 2010) and the code calculations of AISC-LRFD and EC-3 are depicted in Fig. 6 according to FE analysis results. From the comparative results in Table 1, the numerical results were found to be in rather good agreement with the values calculated according to the LTB solution of AISC-

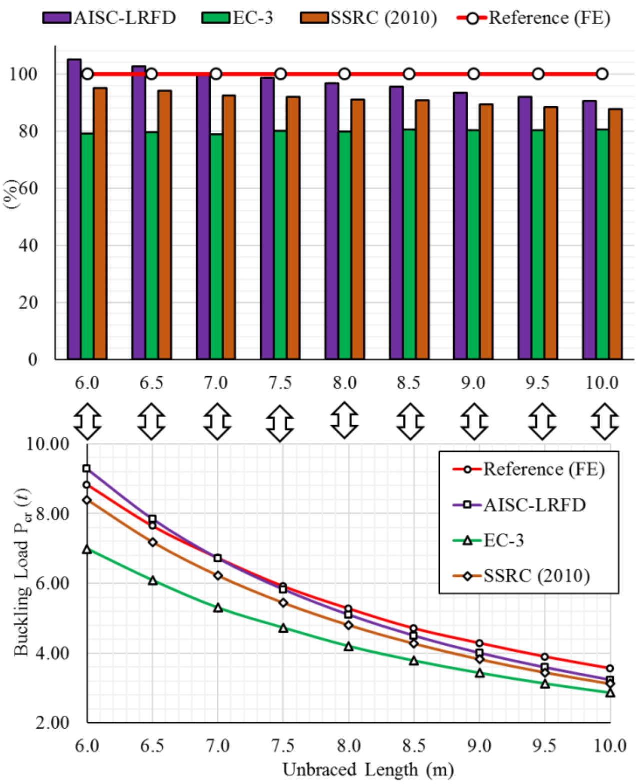

Fig. 6 Variation of the results of numerical (FE) and analytical calculations (AISC-LRFD, EC3 and SSRC, 2010)

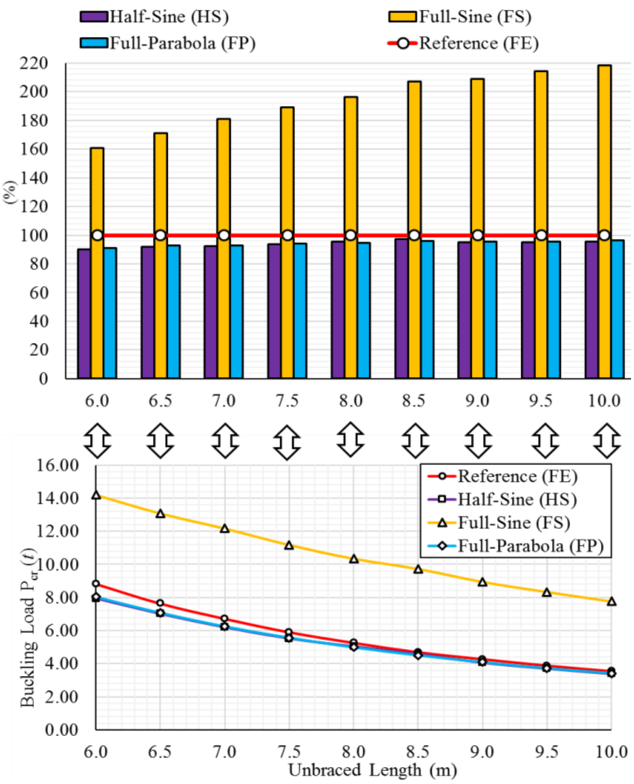

Fig. 7 Variation of the results of numerical (FE) and sweep shapes

Table 2 Comparison between the results of numerical (FE) and sweep shapes

Unbraced length (m)	Reference (FE) $P_{cr,\mathrm{FE}}$	Half-Sine (HS) $P_{cr,\mathrm{HS}}$	HS $P_{cr,\mathrm{HS}}/P_{cr,\mathrm{FE}}$ (%)	HS Decrease (%)	Full-Sine (FS) $P_{cr,\mathrm{FS}}$	FS $P_{cr,\mathrm{FS}}/P_{cr,\mathrm{FE}}$ (%)	FS Increase (%)	Full-Parabola (FP) $P_{cr,\mathrm{FP}}$	FP $P_{cr,\mathrm{FP}}/P_{cr,\mathrm{FE}}$ (%)	FP Decrease (%)
6.0	8.83	7.94	90	-10	14.20	161	61	8.04	91	-9
6.5	7.64	7.02	92	-8	13.08	171	71	7.08	93	-7
7.0	6.72	6.20	92	-8	12.17	181	81	6.25	93	-7
7.5	5.91	5.53	94	-6	11.18	189	89	5.57	94	-6
8.0	5.27	5.04	96	-4	10.35	196	96	4.99	95	-5
8.5	4.70	4.58	97	-3	9.73	207	107	4.51	96	-4
9.0	4.28	4.06	95	-5	8.94	209	109	4.09	96	-4
9.5	3.89	3.70	95	-5	8.33	214	114	3.72	96	-4
10.0	3.56	3.39	95	-5	7.76	218	118	3.42	96	-4

Table 3 Comparison between the results of numerical (FE) and sweep-twist

Unbraced length (m)	Reference (FE) $P_{cr,FE}$	Buckling load (P_{cr}, t) Sweep-twist imperfection: Half-Sine + Twist (HS-T) $P_{cr,HS\text{-}T}$	$P_{cr,HS\text{-}T}/P_{cr,FE}$ (%)	Decrease (%)	Full-Parabola + Twist (FP-T) $P_{cr,FP\text{-}T}$	$P_{cr,FP\text{-}T}/P_{cr,FE}$ (%)	Decrease (%)
6.0	8.83	7.62	86	-14	7.66	87	-13
6.5	7.64	6.69	88	-12	6.73	88	-12
7.0	6.72	5.92	88	-12	5.98	89	-11
7.5	5.91	5.29	90	-10	5.40	91	-9
8.0	5.27	4.75	90	-10	4.85	92	-8
8.5	4.70	4.36	93	-7	4.32	92	-8
9.0	4.28	3.91	91	-9	3.94	92	-8
9.5	3.89	3.57	92	-8	3.58	92	-8
10.0	3.56	3.28	92	-8	3.29	93	-7

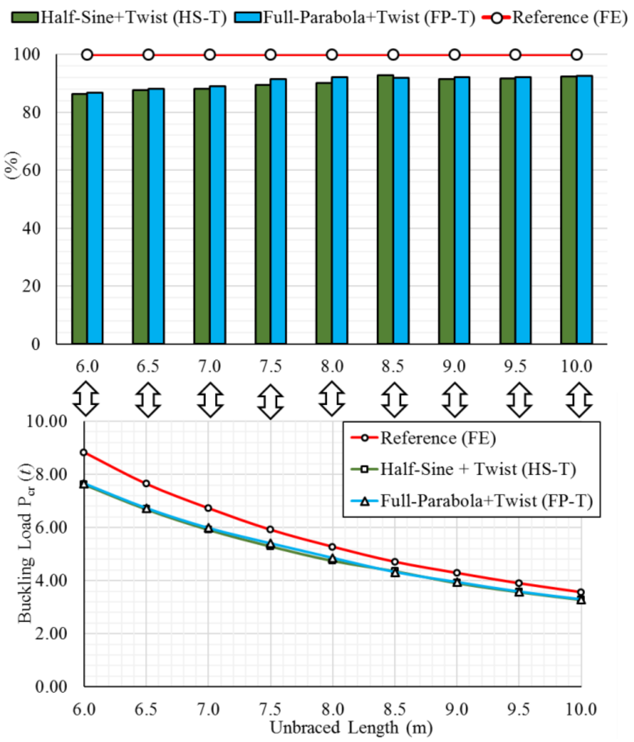

Fig. 8 Variation of the results of numerical (FE) and sweep-twist

LFRD and the theoretical formulation of SSRC (2010). The major differences between the analytical estimates from the EC3 solution and the numerical results imply that the EC-3 formulation given in Eq. (9) predicts the critical loads conservatively. These conservative estimates might stem from the initial imperfection reduction factor (α_{LT}) in the EC-3 formulation (Eq. (9)). On the other hand, lower difference than the EC-3 was shown to be obtained from the theoretical formulation developed from SSRC (2010). The AISC-LFRD formulation also provides much closer estimates to the numerical results than EC3 solution. Consequently, the percent differences from the numerical results can be given as follows: AISC-LRFD (max. 9%), SSRC (2010) (max. 12%) and EC-3 (max. 21%).

4.2 Effect of sweep shapes

The verified FE models of the beams were utilized to determine the influence of the global sweep shapes of half-sine, full-sine and full-parabola on the critical buckling load (P_{cr}). Due to lateral imperfection along the beam, a limited decrease in P_{cr} value was estimated for each sweep shape before the analysis. Accounting for these points, the comparative results are given in Table 2 and depicted in Fig. 7. As in the other estimation, all results were checked in percentage manner against the FE analysis results with respect the reference beams with no imperfection.

The variation of the results from the sweep shapes was also depicted in Fig. 7 according to the reference (FE) outcomes. As clearly demonstrated in Fig. 7, the beams were considerably affected from the full-sine (FS) imperfection with high increase in the Pcr load. This dramatic increase pertained to 2nd buckling mode shapes of the beam. Therefore, the full-sine lateral bow and its derivative forms were decided not to be deemed as an imperfection type for the LTB analysis with the increase in the Pcr reaching to 120%.

As expected, the half-sine (HS) and full-parabola (FP) imperfection shapes caused considerable decrease in the buckling load and these two shapes yielded to relatively comparable results to each other. The maximum decrease in P_{cr} was obtained as 10% and 9% for the half-sine (HS) and full-parabola (FP) imperfection shapes, respectively. So, the beams were understood to be influenced to a higher degree in the case of half-sine sweep than the full-parabola sweep. In general, an imperfect beam can be said to buckle at lower load values as the out-of-plane shape of its longitudinal axis approaches the half sine wave. This conclusion is related to the fact that the longitudinal axis turns into a half-sine wave between the end supports after buckling. Furthermore, the use of different imperfection forms other than the half-sine curve might produce higher buckling load estimates in the design of doubly-symmetric steel I-beam.

4.3 Effect of sweep-twist imperfection

Apart from the initial lateral sweep, another important imperfection relatively effective on the buckling load is the initial angle of twist along the beam. To understand the influence of twist on the buckling behavior, the beams with both sweep and twist imperfection (named sweep-twist imperfection) were analyzed and the comparative results are given in Table 3. For half-sine and twist (HS-T), max. 14% decrease in the buckling load was obtained whereas this decrease was max. 13% for full-parabola and twist (FP-T). It is also interesting to note that for both cases that the percentage decrease in the buckling load increases with decreasing unbraced length (L_b) of the beam.

The differences between the imperfection cases are also seen clearly in Fig. 8. From the Figs. 7 and 8, initial imperfection was determined to be more effective for short beams than long beams. The effect of the twist imperfection on the buckling load was determined through the comparison of the values in Table 2, reflecting the results in the sole presence of sweep, with the values in Table 3, reflecting the results in the simultaneous presence of sweep and twist. Accordingly, the twist with a sinusoidal distribution along the span decreases the buckling load 6% and 4% at greatest for the half-sine and full-parabola shapes of sweep, respectively. This conclusion showed again that half-sine (HS) sweep is a more critical imperfection shape than full-sine parabola.

5. Conclusions

The present study aims to practically identify the influence of the initial imperfection from manufacturing, construction, storage and shipping etc. on the lateral torsional buckling (LTB) behavior of steel I-beams. Different from the previous studies in the literature, the effects of the shape of the initial lateral bow, i.e., the distribution of sweep along the span, on the buckling behavior rather than the amplitude of sweep was investigated. The material imperfection (residual stress) was not considered in this study. For this purpose, a set of IPN300 doubly-symmetric steel I-beams with different unbraced lengths were adopted in the numerical (FE) analyses and analytical calculations according to the code (AISC-LFRD and EC-3) LTB solutions and theoretical formulations (SSRC, 2010). Three shapes of global lateral sweep, namely the full-sine (FS), half-sine (HS) and full-parabola, were used in the analyses both for the presence and absence of initial angle twist with sinusoidal distribution along the span. The maximum sweep value at mid-span (Lb/1000) was kept constant in all imperfection shapes. The FE analyses of the beam with different lengths of 6.0 m, 6.5 m, 7.0 m, 7.5 m, 8.0 m, 8.5 m, 9.0 m, 9.5 m and 10 m were conducted for the following imperfection cases: (i) no imperfection; (ii) only global sweep imperfection; and (iii) sweep-twist imperfection. The results from the last two (ii, iii) imperfection cases were compared to results of the (i) no imperfection case. Based on the comparative results from the numerical and analytical studies, the following conclusions were drawn;

- For eigenvalue elastic buckling response of the beams with no imperfections, EC-3 yielded to more conservative results than the FE analysis, AISC-LRFD and theoretical formulation by SSRC (2010). When compared to the reference (FE) results, AISC-LRFD and theoretical formulation showed a close match. Thus, these formulas can be adopted to reliably predict the elastic eigenvalue LTB of the doubly-symmetric steel I-beams with no initial imperfections.
- The over-conservativity of the EC-3 formulation was estimated to directly originate from the initial imperfection reduction factor in this formulation in its formulation. So, these parameters were stated in the current study to be revised or updated according to various numerical studies.
- Mode-compatible initial imperfection shapes should be taken into account to properly estimate the geometric imperfection influence on the buckling load. The full-sine imperfection shape, which is not compatible to the 1st LTB mode shape of the beam, was found to increase the buckling load, rather than decreasing it.
- Due to the fact that the AISC-LFRD code solution and the theoretical formulation were specified not to consider the effect of geometric imperfection shape (sinusoidal, parabolic, etc.) on the P_{cr} load, the need to develop a practical imperfection reduction factor for AISC-LRFD and theoretical formulation was underlined.
- The beams were determined to be influenced higher in the case of half-sine sweep than full-parabola sweep according to the maximum decrease values in the buckling load, 10% and 9% for the half-sine (HS) and full-parabola (FP) imperfection, respectively. These reductions increase to 14% and 13% in the presence of twist in addition to the half-sine and full-parabola imperfection shapes, respectively.
- According to comparative outcomes, initial imperfections were obtained to be more influential on the buckling load, as the unbraced length of a beam approaches the elastic limit unbraced length (L_r).
- Due to an approximately 15% decrease in the buckling load, the sinusoidal distributions of sweep and twist imperfections is recommended to be considered in the LTB analyses of doubly-symmetric steel I-beams.

Constant values of maximum sweep and initial angle of twist at mid-span were used in the present study for different shapes of initial imperfection. Further studies are recommended to be conducted to assess the influence of the variations in the maximum sweep and twist values together with the shape of lateral imperfection.

References

ABAQUS (2017), Standard User’s Manual; Dassault Systèmes, Waltham, MA, USA.

Agüero, A., Pallarés, L. and Pallarés, F.J. (2015), "Equivalent geometric imperfection definition in steel structures sensitive to flexural and/or torsional buckling due to compression", *Eng. Struct.*, **96**, 160-177.

AISC-LRFD (2016), Specification for structural steel buildings; American Institute of Steel Construction, Chicago, IL, USA.

AS4100-1998 (2016), Steel structures; Standards Association of Australia, Sydney, Australia.

Aydin, R., Gunaydin, A. and Kirac, N. (2015), "On the evaluation of critical lateral buckling loads of prismatic steel beams", *Steel Compos. Struct., Int. J.*, **18**(3), 603-621.

Bas, S., Kalkan, I. and Aykac, S. (2016), "The influence of web distortion of doubly-symmetric steel I-beam on elastic and plastic slenderness limits", *Istanbul Bridge Conference 2016*, Istanbul, Turkey.

Beyer, A., Boissonnade, N., Khelil, A. and Bureau, A. (2018), "Influence of assumed geometric and material imperfections on the numerically determined ultimate resistance of hot-rolled U-shaped steel members", *J. Constr. Steel Res.*, **147**, 103-115.

Chen, G., Zhang, H., Rasmussen, K.J.R. and Fan, F. (2016), "Modeling geometric imperfections for reticulated shell structures using random field theory", *Eng. Struct.*, **126**, 481-489.

Dahmani, L. and Boudjemia, A. (2014), "Lateral torsional buckling response of steel beam with different boundary conditions and loading", *Strength Mater.*, **46**(3), 429-432.

Dou, C. and Pi, Y.-L. (2016), "Effects of geometric imperfections on flexural buckling resistance of laterally braced columns", *J. Struct. Eng.*, **142**(9), 04016048.

Dou, C., Pi, Y.-L. and Gao, W. (2018), "Restraining requirements for lateral elastic-plastic buckling of columns accounting for random imperfections", *Eng. Struct.*, **171**, 260-268.

Eurocode-3 (EC3) (2005), EN 1993-1-1: Design of steel structures - Part 1-1: General rules and rules for buildings European Committee for Standardization; Brussels, Belgium.

Hassan, R. and Mohareb, M. (2015), "Distortional lateral torsional buckling for simply supported beams with web cleats", *Can. J. Civil Eng.*, **42**(12), 1091-1103.

Kala, Z. (2013), "Elastic lateral-torsional buckling of simply supported hot-rolled steel I-beams with random imperfections", *Procedia Eng.*, **57**, 504-514.

Kala, Z. (2017), "Stability of Von-Misses Truss with initial random imperfections", *Procedia Eng.*, **172**, 473-480.

Kala, Z. and Valeš, J. (2017), "Global sensitivity analysis of lateral-torsional buckling resistance based on finite element simulations", *Eng. Struct.*, **134**, 37-47.

Kala, Z., Valeš, J. and Martinásek, J. (2017), "Inelastic finite element analysis of lateral buckling for beam structures", *Procedia Eng.*, **172**, 481-488.

Kalkan, I. and Buyukkaragoz, A. (2012), "A numerical and analytical study on distortional buckling of doubly-symmetric steel I-beams", *J. Constr. Steel Res.*, **70**, 289-297.

Kövesdi, B., Mecséri, B.J. and Dunai, L. (2018), "Imperfection analysis on the patch loading resistance of girders with open section longitudinal stiffeners", *Thin-Wall. Struct.*, **23**, 195-205.

Kuś, J. (2015), "Lateral-torsional buckling steel beams with simultaneously tapered flanges and web", *Steel Compos. Struct., Int. J.*, **19**(4), 897-916

Lei, J.-s. and Li, L.-y. (2017), "Combined web distortional and lateral-torsional buckling of partially restrained I-section beams", *Int. J. Mech. Sci.*, **131-132**, 107-112.

Mirzaie, F., Myers, A.T., Jay, A., Mahmoud, A., Torabian, S., Smith, E. and Schafer, B.W. (2018), "Imperfection measurements to predict buckling behavior of slender steel tubes", *Thin-Wall. Struct.*, **123**, 270-281.

Mohebkhah, A. (2004), "The moment-gradient factor in lateral–torsional buckling on inelastic castellated beams", *J. Constr. Steel Res.*, **60**(10), 1481-1494.

Naderian, H.R., Ronagh, H.R. and Azhari, M. (2014), "Elastic distortional buckling of doubly symmetric steel I-section beams with slender webs", *Thin-Wall. Struct.*, **84**, 289-301.

Nguyen, T.T., Chan, T.M. and Mottram, J.T. (2013), "Influence of boundary conditions and geometric imperfections on lateral–torsional buckling resistance of a pultruded FRP I-beam by FEA", *Compos. Struct.*, **100**, 233-242.

Pezeshky, P. and Mohareb, M. (2014), "Distortional theory for the analysis of wide flange steel beams", *Eng. Struct.*, **75**, 181-196.

Roy, J., Tremblay, R. and Leger, P. (2015), "Torsional effects in symmetrical steel buckling restrained braced frames: evaluation of seismic design provisions", *Earthq. Struct., Int. J.*, **8**(2), 423-442.

Sonck, D. and Belis, J. (2015), "Lateral–torsional buckling resistance of cellular beams", *J. Constr. Steel Res.*, **105**, 119-128.

SSRC (Structural Stability Research Council) (2010), Guide to Stability Design Criteria for Metal Structures; (Edited by R.D. Ziemian), John Wiley & Sons, USA.

Subramanian, L. and White, D.W. (2017), "Flexural resistance of longitudinally stiffened I-girders. II: LTB and FLB limit states", *J. Bridge Eng.*, **22**(1), 04016100.

Subramanian, L. and White, D.W. (2017), "Reassessment of the lateral torsional buckling resistance of I-section members: uniform-moment studies", *J. Struct. Eng.*, **143**(3), 04016194.

Tankova, T., Martins, J.P., Simões da Silva, L., Marques, L., Craveiro, H.D. and Santiago, A. (2018), "Experimental lateral-torsional buckling behaviour of web tapered I-section steel beams", *Eng. Struct.*, **168**, 355-370.

Thai, H.-T., Kim, S.-E. and Kim, J. (2017), "Improved refined plastic hinge analysis accounting for local buckling and lateral-torsional buckling", *Steel Compos. Struct., Int. J.*, **24**(3), 339-349.

Tohidi, S. and Sharifi, Y. (2018), "Flexural distortional strength of steel beams determined by finite-element modelling", *Proceedings of the Institution of Civil Engineers - Structures and Buildings*, **171**(3), 195-202.

Unterweger, H., Taras, A., Loschan, S. and Kettler, M. (2017), "Influence of imperfections on the stability of beams with intermediate flexible supports", *J. Constr. Steel Res.*, **136**, 140-148.

Winkler, R., Kindmann, R. and Knobloch, M. (2017), "Lateral torsional buckling behaviour of steel beams-on the influence of the structural system", *Structures*, **11**, 178-188.

Yang, B., Xiong, G., Ding, K., Nie, S., Zhang, W., Hu, Y. and Dai, G. (2016), "Experimental and numerical studies on lateral-torsional buckling of GJ structural steel beams under a concentrated loading condition", *Int. J. Struct. Stabil. Dyn.*, **16**(1), 1640004.

Zhou, W.-B., Li, S.-J. and Yan, W.-J. (2016), "Practical formulas towards distortional buckling failure analysis for steel–concrete composite beams", *The Struct. Des. Tall Special Build.*, **25**(18), 1055-1072.

Zirakian, T. (2008), "Elastic distortional buckling of doubly symmetric I-shaped flexural members with slender webs", *Thin-Wall. Struct.*, **46**(5), 466-475.

Zirakian, T. and Zhang, J. (2012), "Elastic distortional buckling of singly symmetric I-shaped flexural members with slender webs", *Int. J. Struct. Stabil. Dyn.*, **12**(2), 359-376.

CC